Supporting Information

High Velocity Flows Inside Tube Reactors

Shahana Chatterjee[1,2*], Thomas Abadie[3,4], Meihui Wang[1], Omar K. Matar[3], Rodney S. Ruoff[1,5,6,7*]

1. *IBS Center for Multidimensional Carbon Materials, Ulsan 44919, Republic of Korea*
2. *Make Materials, Toronto, Canada*
3. *Department of Chemical Engineering, Imperial College London, London SW7 2AZ, United Kingdom*
4. *School of Chemical Engineering, University of Birmingham, Birmingham B15 2TT, United Kingdom*
5. *Department of Chemistry, Ulsan National Institute of Science and Technology (UNIST), Ulsan 44919, Republic of Korea*
6. *Department of Materials Science, UNIST, Ulsan 44919, Republic of Korea*
7. *School of Energy and Chemical Engineering, UNIST, Ulsan 44919, Republic of Korea*

chatterjee.shahana@gmail.com, ruofflab@gmail.com, rsruoff@ibs.re.kr

Simulation Details and other Technical Information

Table S-T1. List of symbols.

α/ α_t/ α_{eff}	thermal diffusivity / turbulent thermal diffusivity/ effective thermal diffusivity
δ_{ij}	Kronecker delta
ε/ *epsilon*	specific dissipation rate
g	acceleration due to gravity
k	turbulent kinetic energy per unit mass
K	kinetic energy per unit mass
h	sensible enthalpy per unit mass
I/ I_b	Radiation Intensity/ black body radiation intensity
Ma	Mach number
M_w	molar mass
μ (*mu*)/ μ_t/ μ_{eff}	dynamic viscosity/ turbulent dynamic viscosity/ effective dynamic viscosity
υ / υ_t (*nut*)/ υ_{eff}	kinematic viscosity/ turbulent kinematic viscosity/ effective kinematic viscosity
ω (*omega*)	specific dissipation rate per unit k
p	pressure
p_rgh	hydrostatic pressure
Pr/ Pr_t	Prandtl number/ turbulent Prandtl number
R	gas constant
Re	Reynolds number
R_u	universal gas constant
ρ/ *rho*	density
Sc/ Sc_t	Schmidt number/ turbulent Schmidt number
t	time
T	temperature
Ti	turbulent intensity
τ	shear stress
U	velocity
u_i	velocity component in the i^{th} direction
ξ	vorticity
x_i	i^{th} co-ordinate
Y_i	mass fraction of i^{th} component

System and Measurement Details

Table S-T2. Tube Specifications. ID: Inner Diameter, OD: Outer Diameter, L: Length.

	ID /m	OD /m	L /m	Material
Reactor Tube	0.046	0.0508 (2″)	1.5	Quartz
Reactor Inlet	0.004	Not required	Not required	Stainless steel (SS316)
Reactor Door	Not required	Not required	Not required	Stainless steel (SS316)

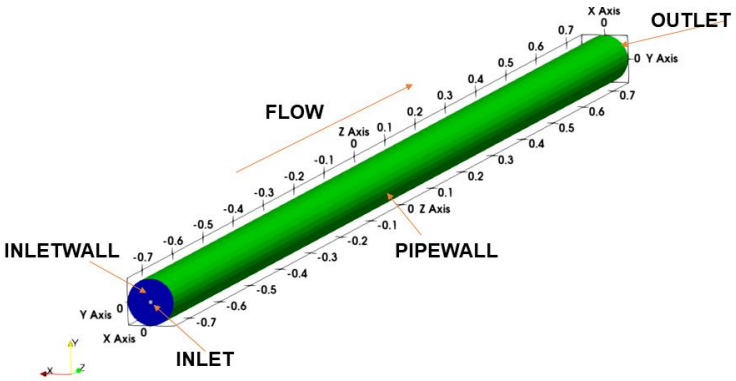

Figure ST-0-A. Details of the tube reactor used for simulations in this paper, based on our CVD system. All axes are in m.

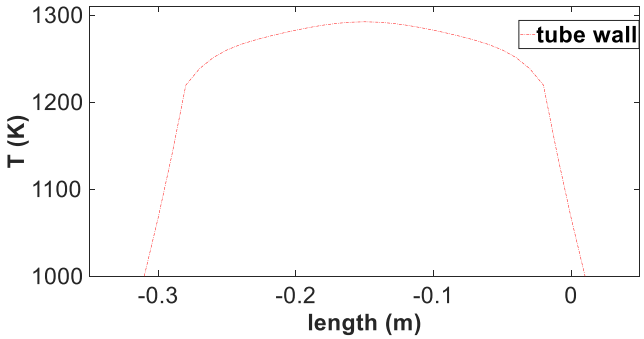

Figure ST-0-B. Thermal profile A centered at z = -0.15 m.

Foil-setups

setup A: at z = -0.15 m, 0.6 m from the inlet centered at y = -0.01090 m
setup B: at z = 0.0 m, 0.75 m from the inlet centered at y = -0.01090 m
All simulations use foil setup A unless otherwise mentioned.

Simulation Details

All solvers discussed below utilize the SIMPLE or SIMPLEC algorithms if steady-state and the PISO or PIMPLE algorithms if transient.[1,2]

Solvers buoyantSimpleFoam (steady-state) and buoyantPimpleFoam (transient). These solvers are used to simulate single-phase flows with low Mach numbers and whose densities change with temperature (and not pressure). In these solvers, the hydrostatic pressure *p_rgh* is used in all equations instead of *p*, where $p\_rgh = p - \rho g h$ **(Eqn1)**.

The following equations are solved:

Momentum equation:

$$\frac{\partial(\rho u_i)}{\partial t} + \frac{\partial(\rho u_j u_i)}{\partial x_j} = -\frac{\partial p_{rgh}}{\partial x_i} + \frac{\partial \tau_{ij}}{\partial x_j} - g x_i \frac{\partial \rho}{\partial x_i}$$

(**Eqn2**), where,

$$\tau_{ij} = 2\mu S_{ij} - \frac{2\mu}{3}(\vec{\nabla}.\vec{V})\delta_{ij}$$

with

$$S_{ij} = \left(\frac{\partial u_i}{\partial x_j} + \frac{\partial u_j}{\partial x_i}\right)$$

Energy equation:

$$\frac{\partial(\rho h)}{\partial t} + \frac{\partial(\rho u_j h)}{\partial x_j} + \frac{\partial(\rho K)}{\partial t} + \frac{\partial(\rho u_j K)}{\partial x_j} - \frac{\partial p}{\partial t} = -\frac{\partial q}{\partial x_j} + \rho r$$

(**Eqn3**) where, *r* is a source term

Continuity equation:

$$\frac{\partial \rho}{\partial t} + \frac{\partial(\rho u_i)}{\partial x_i} = 0$$

(Eqn4)

Solvers chtMultiRegionSimpleFoam (steady-state) and chtMultiRegionFoam (transient). These solvers are used to solve cases where both solid and fluid regions are present. The fluid regions are solved as in the buoyant solvers discussed above. For the solid regions, only an energy equation is solved:

$$\frac{\partial(\rho h)}{\partial t} = -\frac{\partial q}{\partial x_j} + \rho r$$

(Eqn5) where, *r* is a source term

A solid and a fluid region may have a common interface between them. For such interfaces,

$$T_f = (1-f)T_c + f.T_{nbr} + (1-f)grad(T)\delta$$

(Eqn6)

where, T_f is the temperature of the interface, T_c is the temperature of the cell next to it on the fluid side, T_{nbr} is the temperature on the solid side and δ is the distance from the interface of the cell next to it on the fluid side and *f* is a weighting fraction. The last term is dropped when there is no radiative flux.

Radiation Model

As the reactor tube was heated to very high temperatures, effects of radiation had to be included. The radiation model calculated the radiative flux and added it to the energy equation. The FV-DOM or the finite volume discrete ordinates method was used as the radiation model.[3]

This model solves the radiation transport equation for radiation intensity *I*, with varying *I* based on its spatial position $\vec{r}$ as well as its angular direction $\vec{s}$ and time *t*.

$$\frac{1}{c}\frac{\partial I(\vec{r},\vec{s},t)}{\partial t} + \frac{\partial I(\vec{r},\vec{s},t)}{\partial s} = \kappa(\vec{r})I_b(\vec{r},t) - \beta(\vec{r})I(\vec{r},\vec{s},t) + \frac{\sigma(\vec{r})}{4\pi}\int_0^{4\pi} I(\vec{r'},\vec{s},t)\varphi(\vec{s'},\vec{s})d\Omega'$$

(Eqn7)

where, the 1st term on the right-hand side is for absorption with κ as the absorption coefficient, the 2nd term is for emission with β as the emission coefficient, and, the final term is a scattering term with $\varphi(\vec{s'},\vec{s})$ as a phase angle between directions $\vec{s}$ and $\vec{s'}$, and, $\sigma(\vec{r})$ as the out-scattering coefficient. In FV-DOM, this equation is integrated over both a control volume and a control angle Ω.

Turbulence Model

A RANS (Reynolds Averaged Navier Stokes) model has been used to solve for turbulence in the flow. RANS models solve the RANS equations for momentum, energy and species, where averaged values are used instead of instantaneous values. Thus,

$$\frac{\partial(\bar{\rho}\bar{\bar{u}}_i)}{\partial t} + \frac{\partial(\bar{\rho}\bar{\bar{u}}_j\bar{\bar{u}}_i)}{\partial x_j} = -\frac{\partial \bar{p}_{rgh}}{\partial x_i} + \frac{\partial \bar{\tau}_{ij}}{\partial x_j} - \frac{\partial(\bar{\rho}\overline{\overline{u_j''u_i''}})}{\partial x_j} - g x_i\frac{\partial \bar{\rho}}{\partial x_i}$$

(Eqn8)

where $\tilde{u} = \bar{\bar{u}} + u''$ (Favre-averaged) or $u = \bar{u} + u'$ (Reynolds-averaged) with $\tilde{u}$ as the instantaneous value, $\bar{\bar{u}}$, $\bar{u}$ as the average values and u', u'' the fluctuating parts of the variable of interest. The Boussinesq hypothesis corelates $\frac{\partial(\bar{\rho}\overline{\overline{u_j''u_i''}})}{\partial x_j}$ to the turbulent viscosity μ_t and the mean flow velocities. μ_t in the above equations is calculated by solving additional transport equations. These include the transport equation for *k*, where *k* is the specific turbulent kinetic energy. The *k*-ε model is a RANS model that solves a transport equation for ε, the specific dissipation rate while the *k*-ω model is another RANS model that solves a transport equation for ω, the specific dissipation rate per unit k.

k-ε model

Transport equation for *k*:

$$\frac{\partial(\rho k)}{\partial t} + \frac{\partial(\rho u_j k)}{\partial x_j} = \frac{\partial}{\partial x_j}(\mu_{eff,k})\frac{\partial k}{\partial x_j} + P_k - \rho\varepsilon$$

(Eqn9)

Transport equation for ε:

$$\frac{\partial(\rho\varepsilon)}{\partial t} + \frac{\partial(\rho u_j\varepsilon)}{\partial x_j} = \frac{\partial}{\partial x_j}(\mu_{eff,\varepsilon})\frac{\partial \varepsilon}{\partial x_j} + C_{\varepsilon 1}\frac{\varepsilon}{k}P_k - C_{\varepsilon 2}\rho\frac{\varepsilon^2}{k}$$

(Eqn10)

where, $\mu_{eff,k} = \mu + \frac{\mu_t}{\sigma_k}$, and, $\mu_{eff,\varepsilon} = \mu + \frac{\mu_t}{\sigma_\varepsilon}$ with $C_{\varepsilon 1}$ =1.44, $C_{\varepsilon 2}$ = 1.92, σ_k = 1.0, σ_ε = 1.3

k-ω model

Transport equation for *k*:

$$\frac{\partial(\rho k)}{\partial t} + \frac{\partial(\rho u_j k)}{\partial x_j} = \frac{\partial}{\partial x_j}(\mu_{eff,k})\frac{\partial k}{\partial x_j} + P_k - \beta^*\rho k\omega$$

(Eqn11)

Transport equation for ω:

$$\frac{\partial(\rho\omega)}{\partial t} + \frac{\partial(\rho u_j\omega)}{\partial x_j} = \frac{\partial}{\partial x_j}(\mu_{eff,\omega})\frac{\partial \omega}{\partial x_j} + C_{\alpha 1}\frac{\omega}{k}P_k - C_{\beta 1}\rho\omega^2$$

(Eqn9)

where, $\mu_{eff,k} = \mu + \frac{\mu_t}{\sigma_k}$, and, $\mu_{\text{eff},\omega} = \mu + \frac{\mu_t}{\sigma_\omega}$ with $C_{\alpha 1}$ =5/9, $C_{\beta 1}$ = 0.075, σ_k = 2, σ_ω = 2.

The model that has been used for this work is the *k-ω* SST (shear stress transport) model that blends the *k-ε* and the *k-ω* models. This model uses a viscosity limiter for calculating the viscosity at the wall and thus, does not overestimate the wall shear stress and is better at predicting flow separation under adverse pressure gradients, which is what occurs in the reactor tube. It uses the *k-ε* model for regions of high *Re* in the center of the tube and the *k-ω* model for regions near the walls, because of their better accuracies in these regions of the tube. υ_t is calculated as:
k-ε model: $\upsilon_t = C_\mu \frac{k^2}{\varepsilon}$ with $C_\mu = 0.09$; *k-ω* model: $\upsilon_t = \frac{k}{\omega}$ and used in the RANS equations.

Wall Functions. All meshes used had average *yPlus* values < 1 at the walls (reactor walls, copper foil). Hence, for *k*, a fixed value of 0 was used at the walls. *yPlus* was calculated as $y^+ = \frac{\rho * y * u_T}{\mu}$, where, u_T is the friction velocity and *y* is the wall normal distance, and, $u_T = C_\mu^{0.25} k^{0.5}$. The nutkWallFunction set the values of $\upsilon_t = 0$ in the viscous sub-layer and $\upsilon_t = \upsilon_{lam}\left(\frac{\kappa * y^+}{ln(Ey^+)} - 1\right)$ in the log-law layer with the von Kármán constant κ = 0.41. For ω, the omegaWallFunction discontinuously switched the ω value in the viscous sub-layer and the log-law layer. Thus, $\omega = \frac{6 * \upsilon_{lam}}{\beta_1 * y^2}$ in the viscous sub-layer and $\omega = \frac{\sqrt{k}}{C_\mu * \kappa * y}$ with β_1 = 0.075 in the log-law layer. For turbulent thermal diffusivity α_t, the alphatWallFunction was used, which calculated $\alpha_t = \frac{\rho \upsilon_t}{Pr_t}$ with Pr_t being the turbulent Prandtl number. Following Reynolds analogy, Pr_t for the internal field was set to 1.0.

Thermophysical Properties

All gases have been assumed to be perfect gases. Their viscosities and heat capacities (C_p) have been considered to be temperature dependent ('sutherland' and 'janaf' types respectively). Emissivity of Ar and H_2 are 0.0.[4] For multicomponent fluids (Ar-H_2 mixtures), molecular weights, janaf coefficients and viscosity were calculated from the values for Ar and H_2.

For Ar, H_2 and CH_4, laminar or molecular Prandtl numbers (*Pr*) of 0.67, 0.69 and 0.72 were used. All laminar or molecular Schmidt number (*Sc*) values were set to 1.0.

For solid copper, thermophysical properties at ~1000 °C were used, when the average temperature of the copper foil was around this temperature.[5,6] Alternately, for wider ranges of temperature, temperature dependent values of thermal conductivity and heat capacity have been used for both the copper foil and the stainless-steel thermocouple thermometer.

Calculating Fluid Averages

All fluid average values were calculated for a 2 cm long (*z*) region centered at the hot-zone center (and around the foil when present).

Mesh Details

The mesh had two regions, a solid region for the foil and a fluid region for process gases. All meshing was done using snappyHexMesh.

Table S-T3. Mesh Details.

	100 μm Foil				50 μm Foil
Number of Cells	Mesh 1	Mesh 2	Mesh 3 (default)	Mesh 4	Mesh50
Fluid Region	1706019	3760310	4165275	5516104	7093699
Solid Region	33280	33280	74496	74496	132608

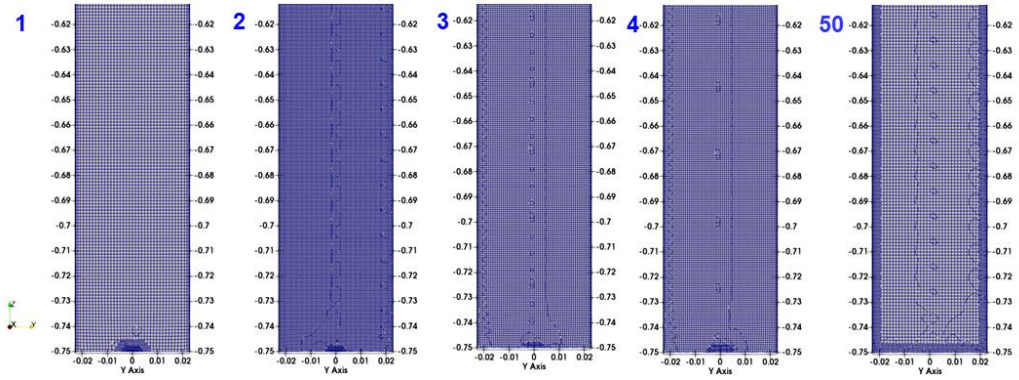

Figure S-T2A. *YZ* slices (at x = 0 m) showing the entrance regions for meshes 1 – 4, mesh50. Axes grid is in m.

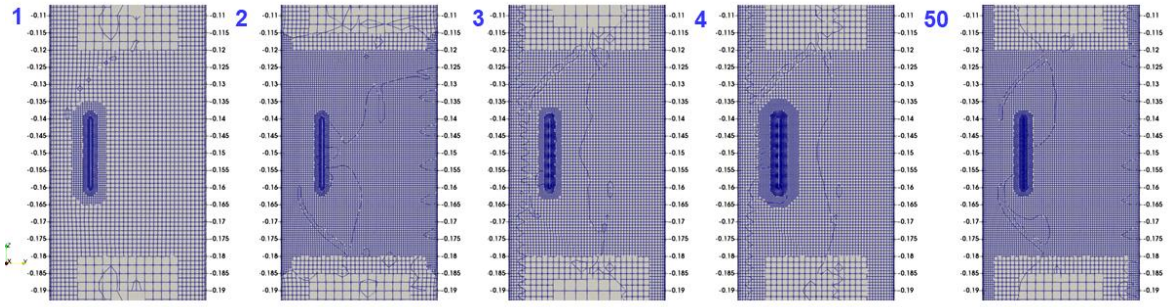

Figure S-T2B. *YZ* slices (at x = 0 m) showing the region surrounding the foil for meshes 1 – 4, mesh50. Axes grid is in m.

Effect of foil position along the *y* axis (i.e. in the vertical direction, 100 µm foil, setup A, condition T0)

An effect that was observed slightly downstream to the foil was asymmetric maxima in the line profiles of variables such as *k*, *ε* and *Ti* (with their respective maxima on the positive y side being taller). This is a result of the flow being diverted away from the foil and the foil being positioned in the lower half of the tube (in comparison, if the foil was placed right at the center (at *y* = 0) of the reactor tube, peak symmetry was found to have been restored).

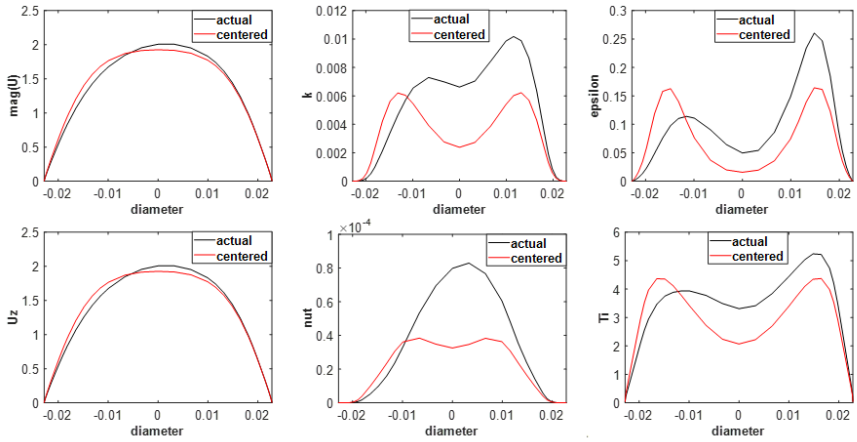

Figure S-T3. Line profiles along the tube *y* diameter (m) at *x* = 0 m and downstream to the foil (at *z* = 0.2 m), comparing a reactor tube with a foil at *y* = -0.0109 m (actual, **setup A**) with a tube with a foil at *y* = 0.0 m (centered). mag(*U*), U_z are in ms^{-1}, *k* is in m^2s^{-2}, *nut* (υ_t) is in m^2s^{-1}, *epsilon* (*ε*) is in m^2s^{-3}, and, *Ti* has been expressed as a %. Both tubes are at RT (**condition T0**).

Buoyancy Effect for Heated Tubes

Line profiles for *k*, *ε* and *Ti* across the *x* diameter of the tube downstream to the hot-zone showed symmetric maxima, while those across the *y* diameter showed asymmetric peaks with the taller peaks on the lower temperature or higher density and lower viscosity side (**Figure S-T6**). The observed asymmetry is an effect of buoyancy, with the acceleration due to gravity *g* acting in the negative *y* direction and hotter gas with lower density moving upwards.

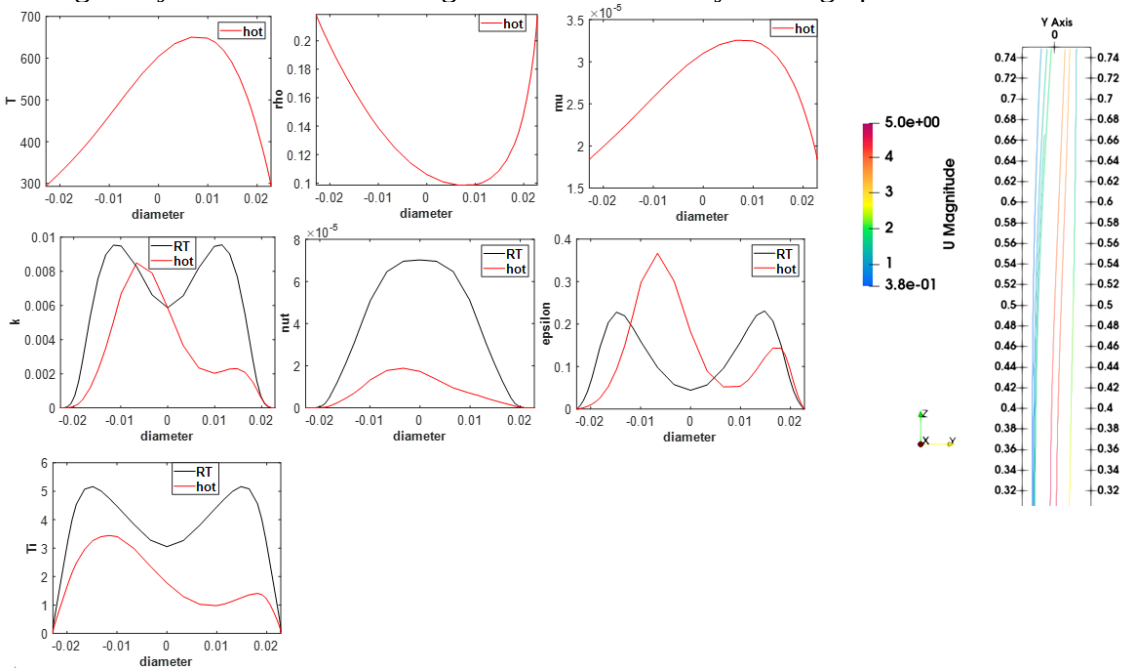

Figure S-T6. Line profiles along the tube *y* diameter (m) at $x = 0$ m and downstream to the hot-zone center (at $z = 0.6$ m), comparing an empty reactor tube at RT (**condition T0**) and a hot and empty reactor tube (**condition T1**). *T* is in K, *rho* is in kgm^{-3}, *mu* (μ) is in $kgm^{-1}s^{-1}$, *k* is in m^2s^{-2}, *nut* (υ_t) is in m^2s^{-1}, and, *epsilon* (ε) is in m^2s^{-3}, *Ti* has been expressed as a %. The figure on the right show the bending of streamlines in the positive *y* direction because of buoyancy, downstream to the hot-zone center. All axes are in m.

Mesh Dependency Study

The dependency of the results obtained on the mesh was tested with four different meshes (**Table S-T3**, with the 100 μm foil); a coarse mesh, two medium meshes, and a fine mesh. All trends were similar and the values obtained were very close.

Table S-T4. Comparison (of fields around the foil) between different meshes for Ar only flows for a heated reactor (**setup A**, **condition T1**) with 100 μm foil.

	T_{foil}, min (K)	T_{foil}, max (K)	T_{foil}, avg (K)	T_{gas}, min (K)	T_{gas}, max (K)	T_{gas}, avg (K)
Mesh 1	1203.61	1292.3	1246.19	393.225	1292.3	737.259
Mesh 2	1202.12	1292.3	1245.37	391.16	1292.3	727.054
Mesh 3 (default)	1202.51	1292.3	1245.54	392.694	1292.3	722.249
Mesh 4	1202.18	1292.3	1245.34	394.313	1292.3	722.705

	U, avg (ms^{-1})	k, avg (m^2s^{-2})	Ti, avg (%)
Mesh 1	3.540	0.00763875	2.016
Mesh 2	3.491	0.00773358	2.054
Mesh 3 (default)	3.492	0.00791561	2.080
Mesh 4	3.484	0.00775683	2.062

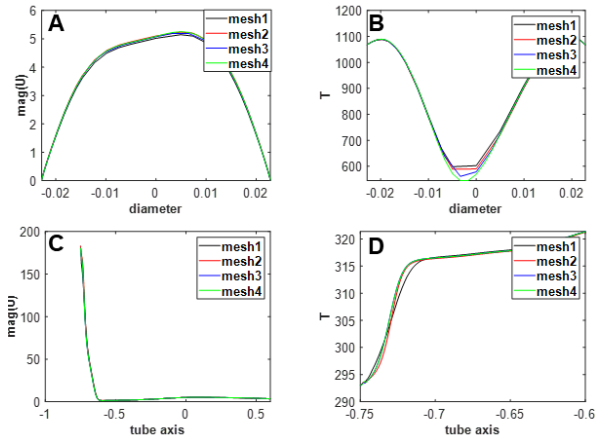

Figure S-T7. Line profiles for U (ms^{-1}) and T (K) along (A), (B) y diameter (m) at x = 0 m and at z = 0.0 m, and, (C), (D) tube axis (m) obtained for different meshes with 100 μm foil (**setup A**, **condition T1**).

Dependency on Pr_t

For gases, a turbulent prandtl number Pr_t, such as 0.7 or 0.85 are often used. Though the temperatures obtained with Pr_t 0.7 or 0.85 (**Table S-T5**, **Figure S-T8**) were very similar to the default Pr_t of 1, a slight increase in temperature was observed with decreasing Pr_t. This also meant a slight increase in velocity and lower turbulence intensities.

Table S-T5. Comparison between different values of Pr_t (of fields around the foil).

Pr_t	T_{foil}, min (K)	T_{foil}, max (K)	T_{foil}, avg (K)	T_{gas}, min (K)	T_{gas}, max (K)	T_{gas}, avg (K)
1.0	1202.51	1292.3	1245.54	392.694	1292.3	722.249
0.85	1202.99	1292.3	1245.78	398.632	1292.3	723.736
0.7	1203.54	1292.3	1246.05	406.362	1292.3	725.635

Pr_t	U, avg (ms^{-1})	k, avg (m^2s^{-2})	Ti, avg (%)
1.0	3.492	0.00791561	2.080
0.85	3.497	0.00790055	2.074
0.7	3.506	0.00788054	2.065

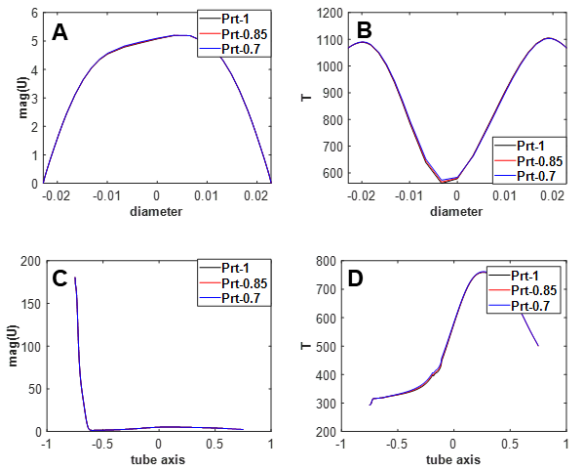

Figure S-T8. Line profiles for U(ms^{-1}) and T(K) along (A), (B) y diameter (m) at x = 0 m and at z = 0.0 m, and, (C), (D) tube axis (m) obtained for different Pr_t with the 100 μm foil (**setup A**, **condition T1**).

Alternate Method for Calculating Turbulent Intensity at Inlet

Simulations were performed by using a different *Ti* calculation method at inlet: $Ti = 0.055Re^{-0.041}$ with the 100 μm foil (**setup A**, **condition T1**). Very little difference was observed in the resulting fields.

Table S-T6. Simulations with different values of turbulent intensity at inlet (of fields around the foil).

Ti at inlet	T_{foil}, min (K)	T_{foil}, max (K)	T_{foil}, avg (K)	T_{gas}, min (K)	T_{gas}, max (K)	T_{gas}, avg (K)
5.4% (default)	1202.51	1292.3	1245.54	392.694	1292.3	722.249
3.9%	1202.61	1292.3	1245.59	393.219	1292.3	722.552

Ti at inlet	*U*, avg (ms^{-1})	*k*, avg (m^2s^{-2})	*Ti*, avg (%)
5.4% (default)	3.492	0.00791561	2.080
3.9%	3.492	0.00798554	2.089

Table S-T7. Details of boundary conditions used for different fields, for single-region cases or the fluid regions of multi-region cases

	inlet	outlet	walls (of pipe and foil)
U	codedFixedValue with power-law velocity profile (n = 6) with time ramp	inletOutlet	fixedValue; uniform (0 0 0)
k	turbulentIntensityKineticEnergyInlet	inletOutlet	fixedValue; uniform 0
omega	fixedValue (calculated with average U)	inletOutlet	omegaWallFunction
nut	calculated	calculated	nutkWallFunction
alphat	calculated	calculated	compressible alphatWallFunction
p_rgh	fixedFluxPressure	fixedValue (100 torr)	fixedFluxPressure
p	calculated	calculated	calculated
T	fixedValue (293 K)	inletOutlet	single-region cases at RT: zeroGradient pipe wall at high temperatures: fixed value with thermal profile A; foil at high temperatures and multi region cases: mapped wall with turbulentTemperatureRadCoupledMixed
IDefault	greyDiffusiveRadiation	greyDiffusiveRadiation	greyDiffusiveRadiation

Figures supplementing the Main Text

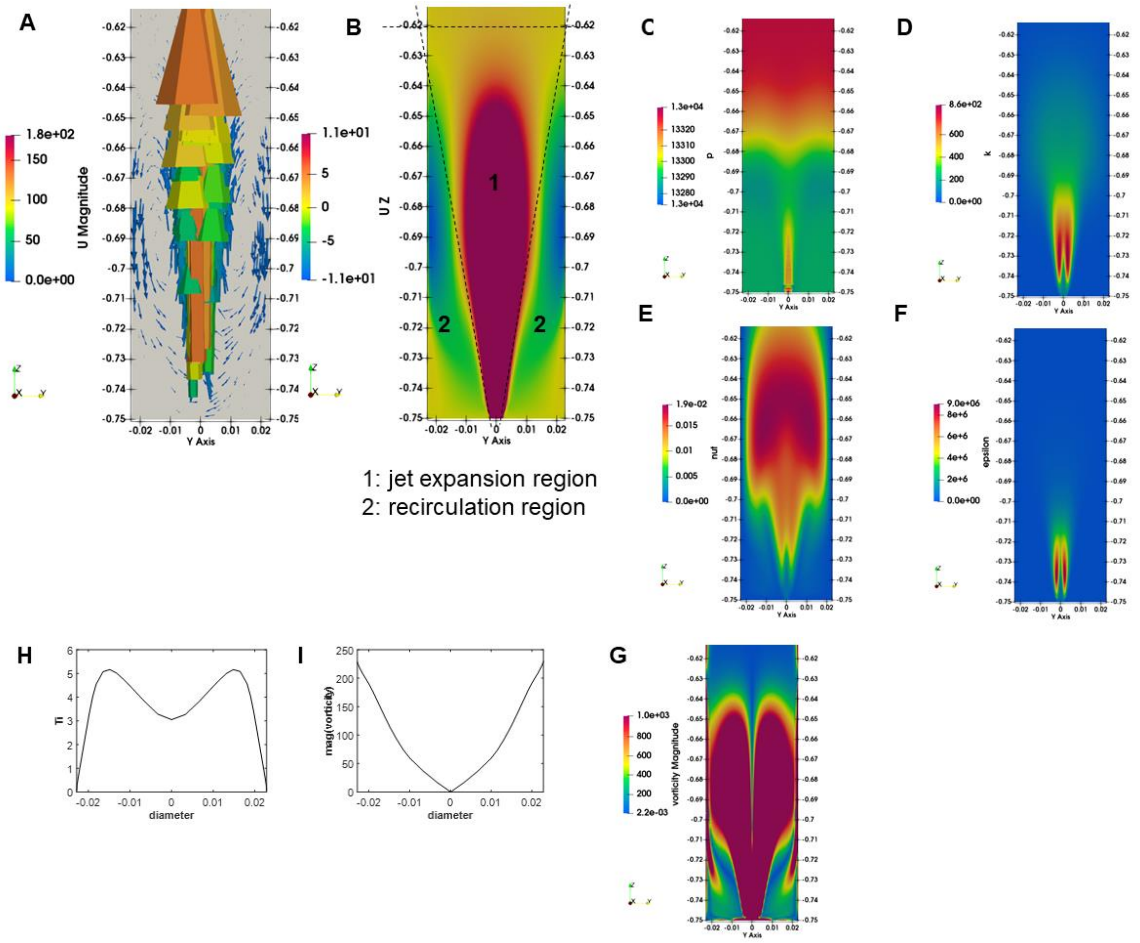

Figure S1. Entrance region for an Ar flow at 100 torr at RT (**condition T0**) into the reactor tube with no foil. *YZ* slice (axes in m, at x = 0) through the tube showing (A) velocity vectors for mag(*U*), and, (B) *Uz*, (C) *p*, (D) *k*, (E) *nut* (υ_t), (F) *epsilon* (ε) fields and, the magnitude of vorticity. (H)-(I) line profiles across the tube *y* diameter (m) at x = 0 m and for Ti (%) and the magnitude of vorticity (s^{-1}) at z = 0.6 m. mag(*U*), U_z are in ms^{-1}, *p* is in Pa, *k* is in m^2s^{-2}, *nut* is in m^2s^{-1}, *epsilon* is in m^2s^{-3}, and, the magnitude of vorticity is in s^{-1}.

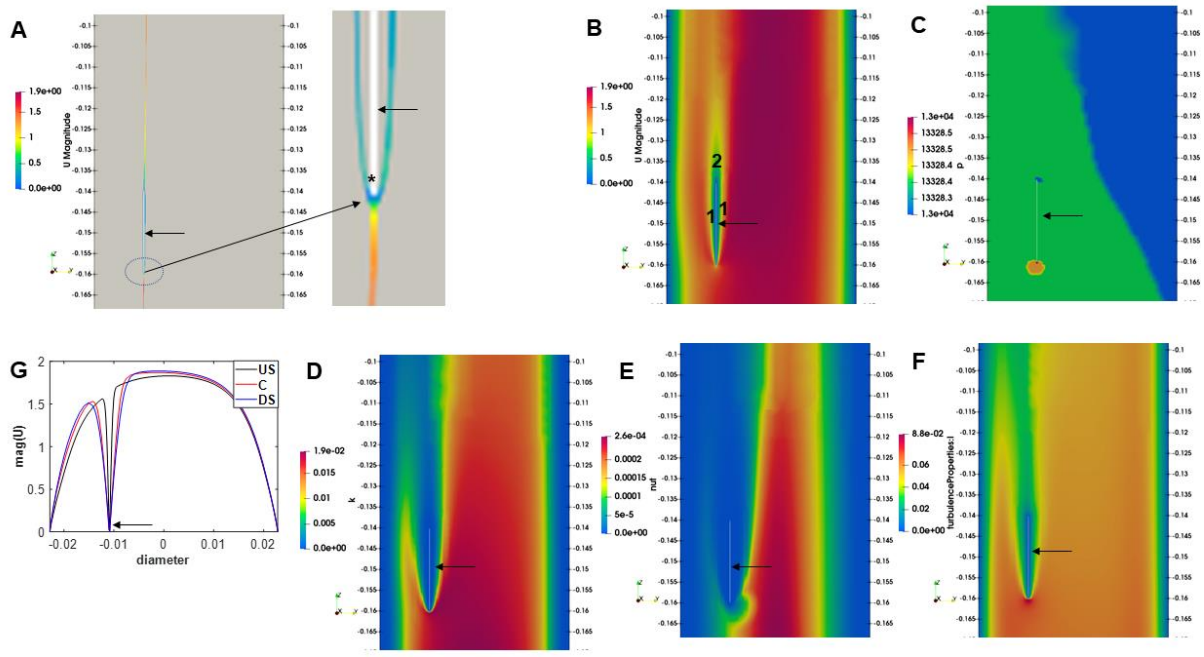

Figure S2. An Ar only flow at 100 torr at RT (**condition T0**) into the reactor tube with a 100 μm foil. Arrows indicate the foil position. *YZ* slices (axes in m, at x = 0 m) showing (A) streamlines around the foil showing a stagnation line *, (B) mag(U), (C) p, (D) k, (E) *nut* (υ_t), (F) *Ti* fields. In (B) regions marked as (1) are the boundary layer (BL) regions around the foil while (2) is the wake region downstream to the foil. (G) shows line profiles along the y diameter (m) of the tube at x = 0 m for mag(U), close to the foil upstream edge (US at z = -0.159 m), the foil center (C at z = -0.15 m), and close to the foil downstream edge (DS at z = -0.141 m). mag(U), U_z are in ms^{-1}, p is in Pa, k is in m^2s^{-2}, *nut* (υ_t) is in m^2s^{-1}, *epsilon* (ε) is in m^2s^{-3}.

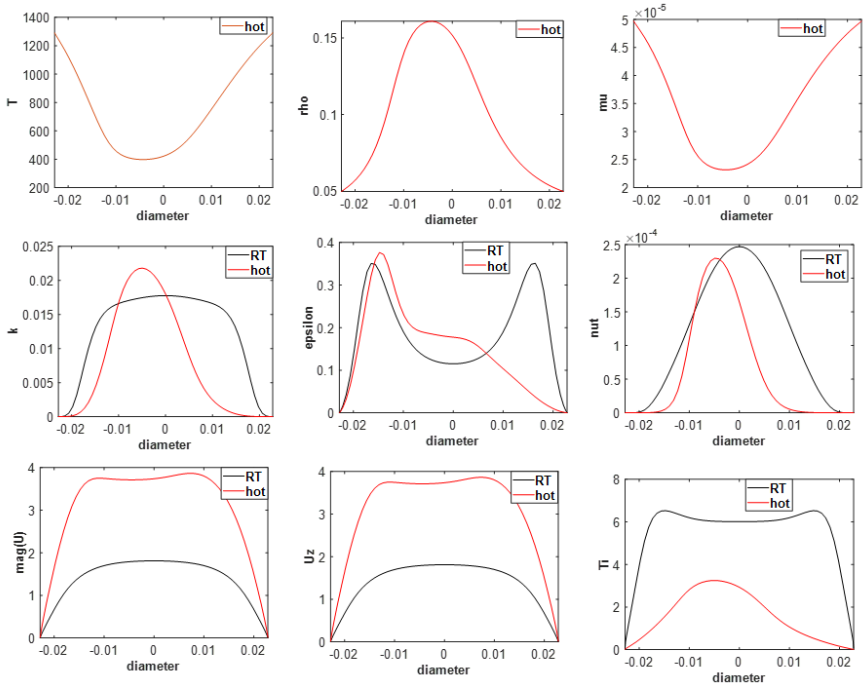

Figure S3. Line profiles along the tube *y* diameter (m) at x = 0 m and at the center of the hot zone for an empty reactor tube, compared with an empty tube at RT. T in in K, *rho* is in kgm^{-3}, *mu* (μ) is in $kgm^{-1}s^{-1}$, k is in m^2s^{-2}, *epsilon* (ε) is in m^2s^{-3}, *nut* (υ_t) is in m^2s^{-1}, mag(U), U_z are in ms^{-1}, and, *Ti* has been expressed as a %.

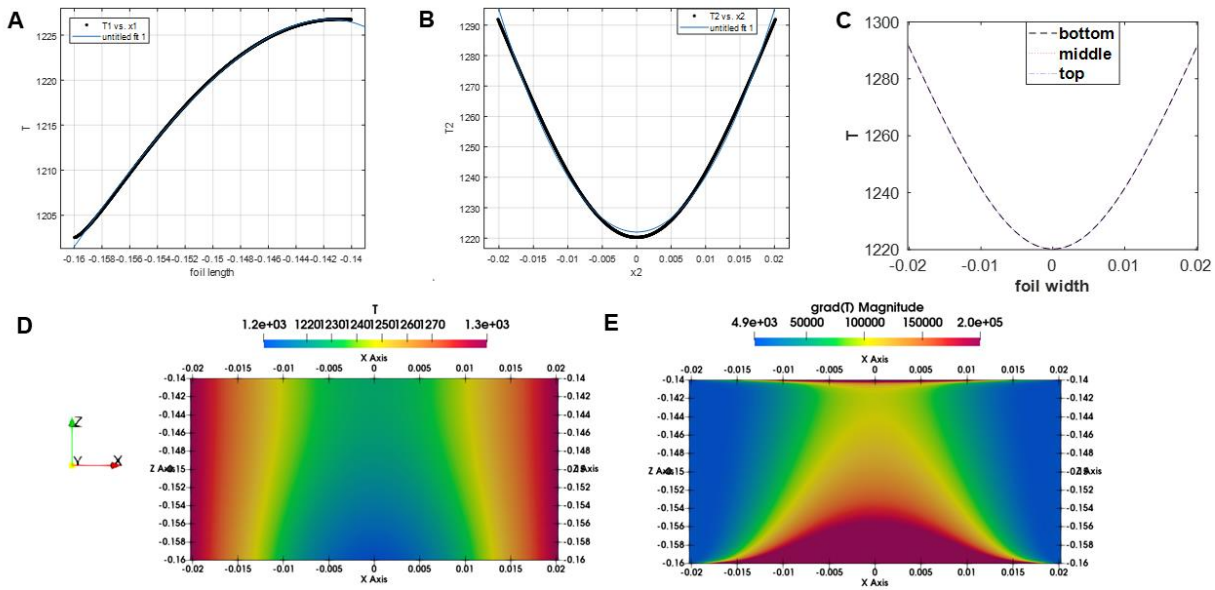

Figure S4. Line profiles across the foil (100 μm, **setup A** and **condition T1**) showing (A) an exponential increase in *T* (K) along the foil length (m) from the upstream to the downstream edge through its middle (along *z* at *x* = 0 m, *y* = -0.0109 m), and, (B) across the foil width (m, along *x*, at *y* = -0.0109 m, *z* = -0.15 m) showing a parabolic shape. (C) shows three-line profiles for *T* (K) across the foil width (m, along *x* at *z* = -0.15 m), one close to the bottom surface (*y* = -0.01094 m), one through the middle of the foil (*y* = -0.0109 m) and one close to the top surface of the foil (*y* = -0.01086 m). (E) and (F) show the *T* (K) and *grad(T)* (Km^{-1}) on the bottom surface of the foil (axes in m) .

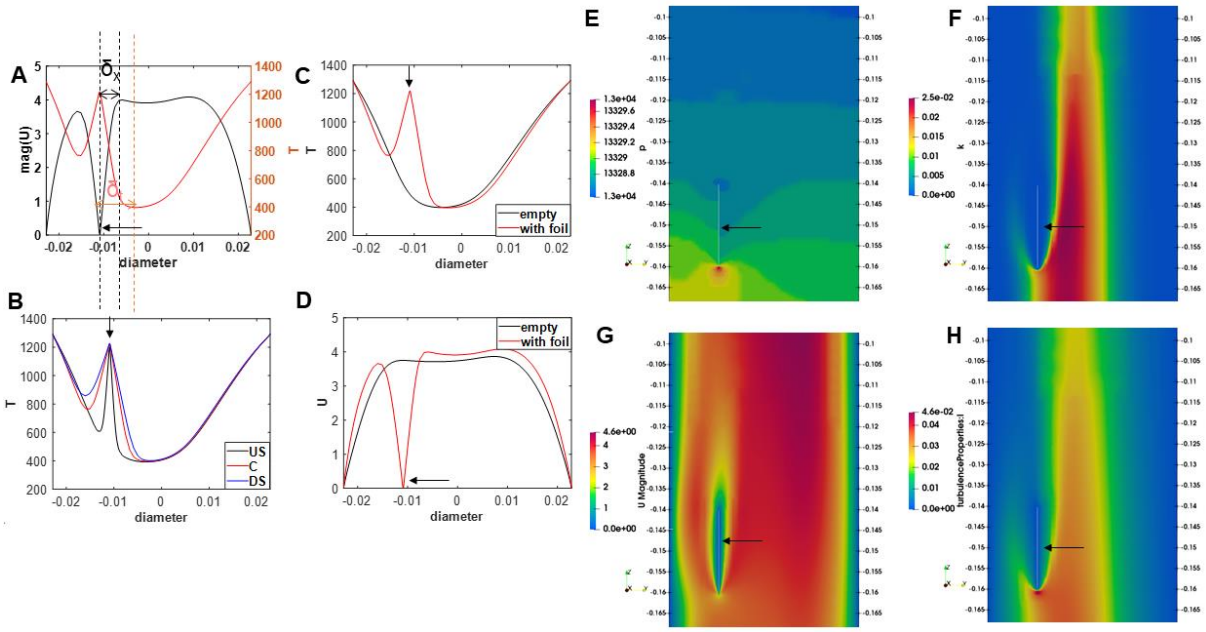

Figure S5. Heated reactor tube with 100 μm foil (**setup A** and **condition T1**). Arrows indicate foil position. Line profiles along the tube *y* diameter (m) at $x = 0$ m and across the foil: (A) showing mag(*U*) and *T* profiles across the foil center ($z = -0.15$ m); (B) comparison of profiles across the upstream edge (US), center (C) and downstream edge of the foil (DS) for *T* (K); comparison of the line profiles across the foil center with an empty heated tube: (C) *T* and (D) mag(*U*). (E)-(H) *YZ* slices (axes in m, at $x = 0$ m) across the tube showing different fields around the foil: (E) *p* (Pa), (F) *k* (m^2s^{-2}), (G) mag(*U*) (ms^{-1}), and, (H) *Ti*.

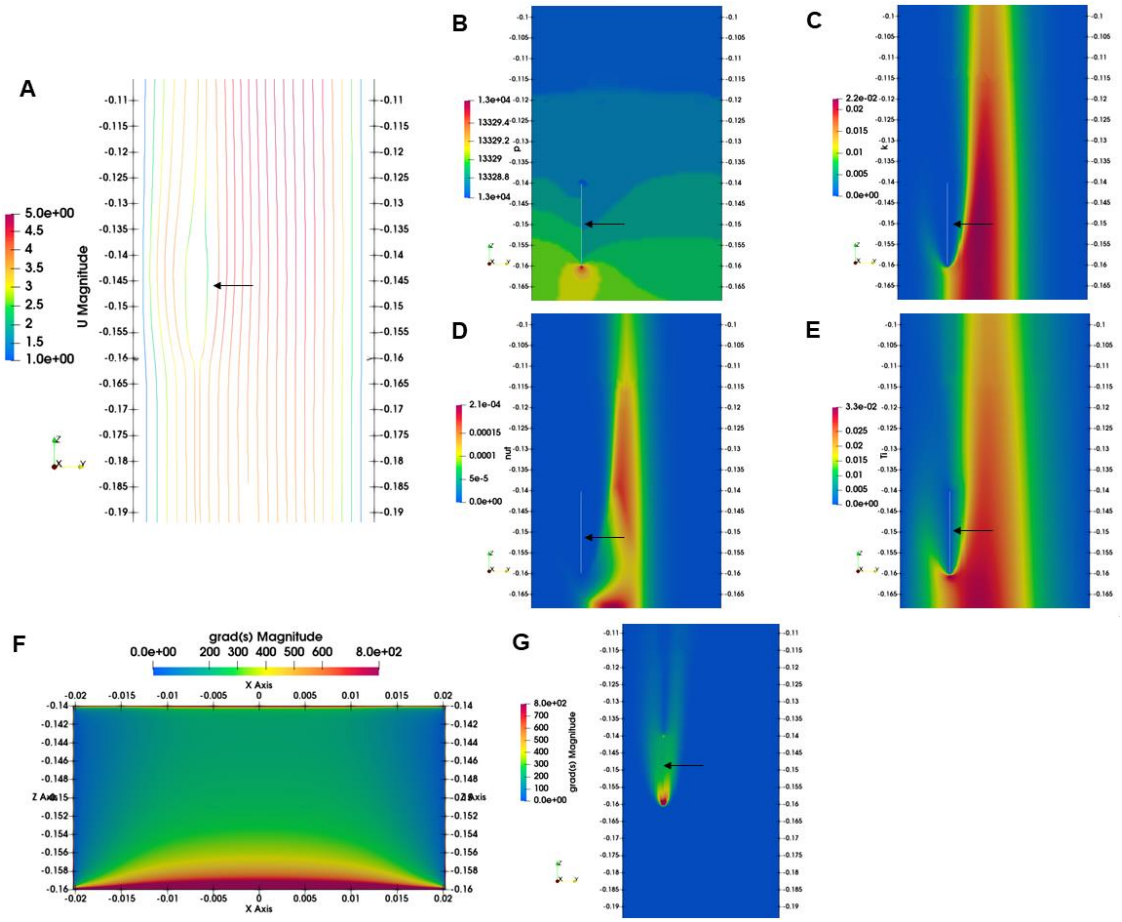

Figure S6. *YZ* slice (axes in m, at x = 0 m) of the reactor tube showing (A) streamlines (color coded with U_{mag} in ms^{-1}), (B) p (Pa), (C) k (m^2s^{-2}), (D) *nut* (υ_t) (m^2s^{-1}), (E) *Ti*, and, (G) normalized CH_4 concentration gradient (*grad(s)*) around the 50 µm foil (**setup A**, **condition A**). (F) shows the normalized CH_4 concentration gradient (*grad(s)*) on the foil surface (axes in m). Arrows indicate foil location. Arrows indicate foil location.

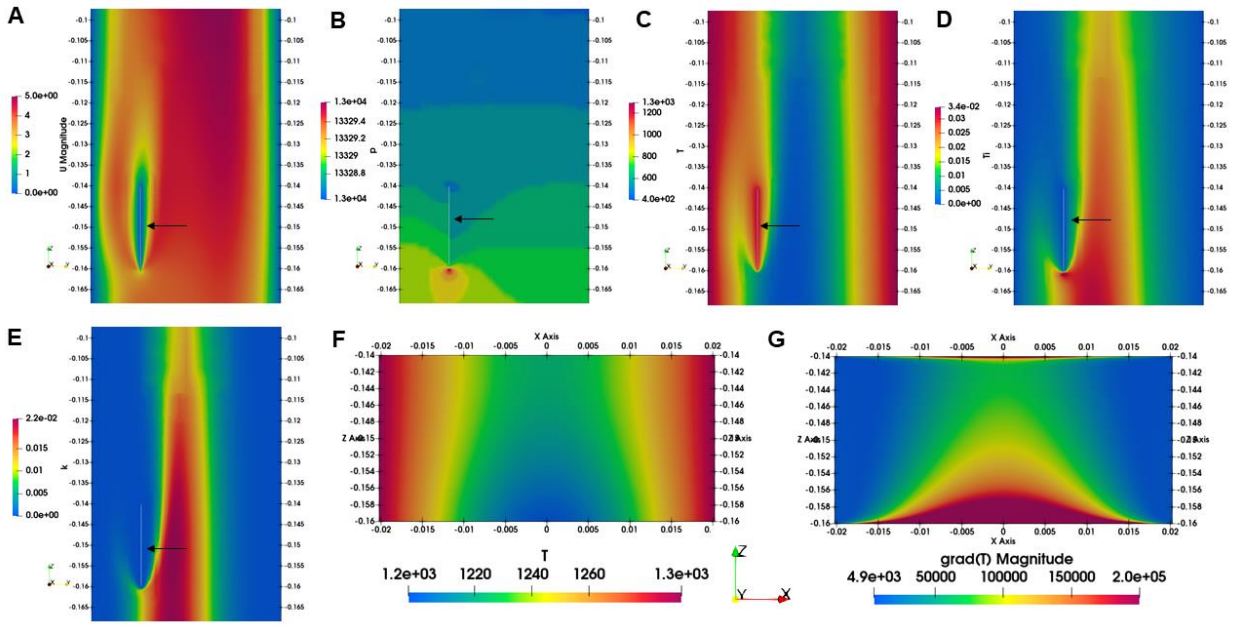

Figure S7. Heated reactor tube with a 100 μm foil with **foil setup A** and **condition A**. (A)-(E) are *YZ* slices (axes in m, at x = 0 m) of the reactor tube showing different flow fields around the foil: (A) mag(U) (ms^{-1}), (B) p (Pa), (C) T (K), (D) Ti, (E) k (m^2s^{-2}). (F) and (G) show the T (K) and the *grad(T)* (Km^{-1}) on the foil surface (axes in m). Arrows indicate foil location.

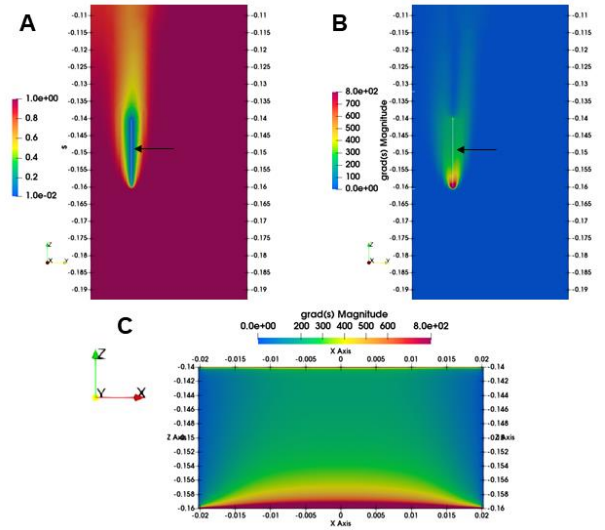

Figure S8. *YZ* slice (axes in m, at x = 0 m) of the reactor tube showing normalized (A) CH_4 (*s*) concentration and (B) concentration gradient (*grad(s)*) around the foil; (C) shows *grad(s)* on the foil surface (axes in m) for a heated reactor tube with a 100 μm foil with **foil setup A** and **condition A**. Arrows indicate foil location.

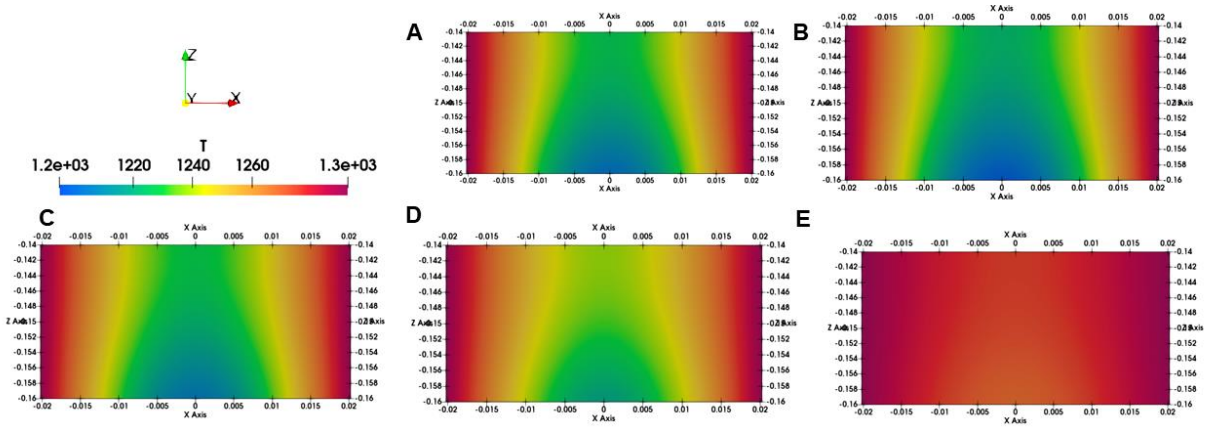

Figure S9. *T* (K) of foil surfaces (axes in m) for 100 μm foils (with **foil setup A**) for flows with different mass% of H_2: (A) an Ar only flow, flows with (B) 1%, (C) 10%, and, (D) 15% H_2 and, (E) a H_2 only flow.

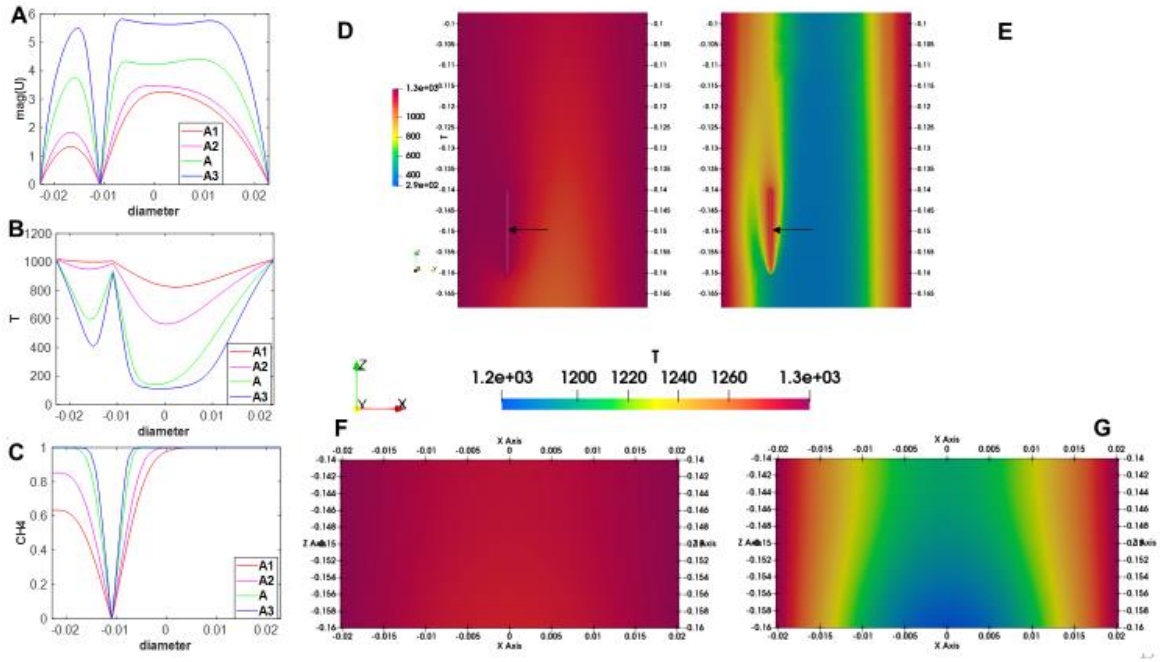

Figure S10. (A)-(C) Line profiles along the tube *y* diameter (m) at x = 0 m and across the center (at z = -0.15 m) of the 100 μm foil (with **foil setup A**) for different flow velocities and Ar proportions (both increase in order of A1, A2, A and A3): (A) mag(U) (ms^{-1}), (B) T (K), (C) normalized CH_4 concentration. (D)-(E): *YZ* slices (axes in m, at x = 0 m) through the reactor tube showing gas T (K) around the foil for: (F) A1, and, (G) A3. (G)-(H): Foil surface (axes in m) T (K) for (H) A1, and, (I) A3. Arrows indicate foil location.

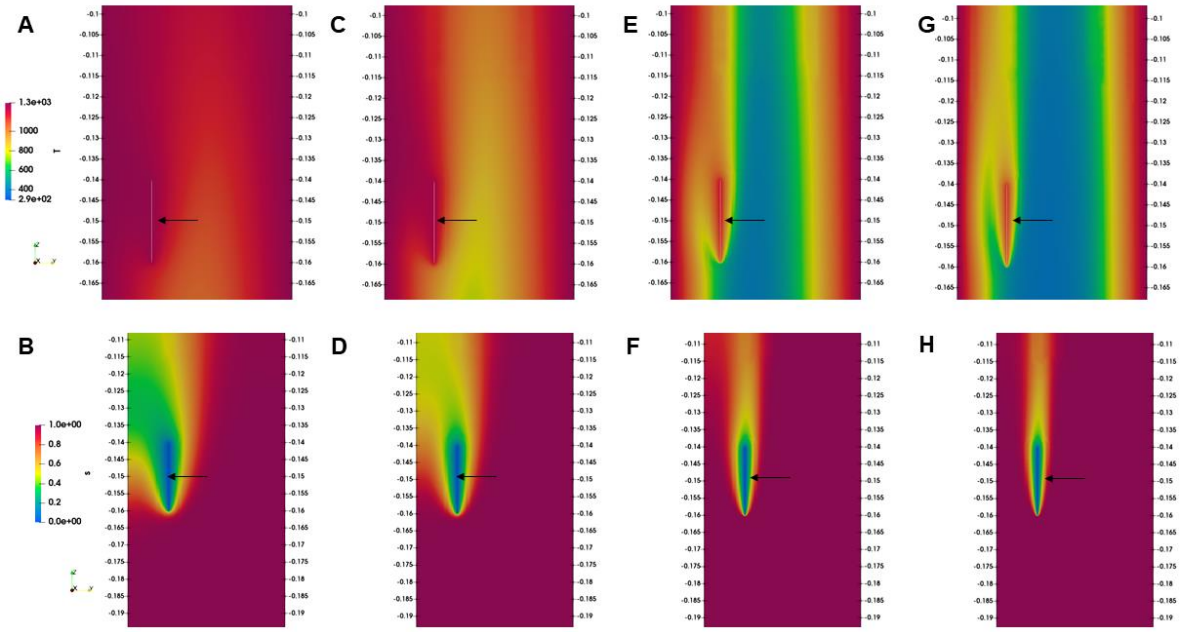

Figure S11. *YZ* slices (axes in m, at x = 0 m) through the reactor tube showing gas T (K) and normalized CH_4 distribution (s) around the 50 μm foil for process: (A)-(B) A1, (C)-(D) A2, (E)-(F) A, (G)-(H) A3. Arrows indicate foil location.

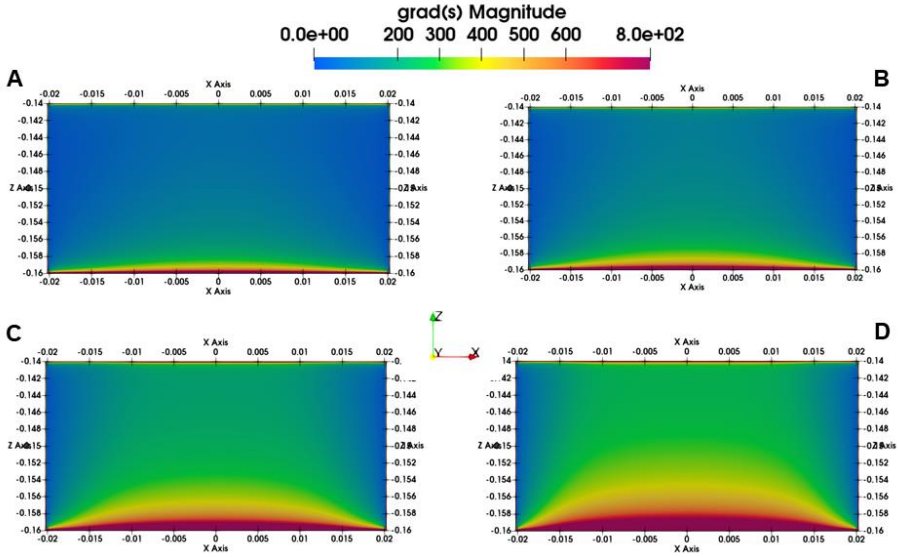

Figure S12. Normalized CH_4 concentration gradients (grad(s)) on the 50 μm foil surface (axes in m) for process: (A) A1, (B) A2, (C) A, (D) A3.

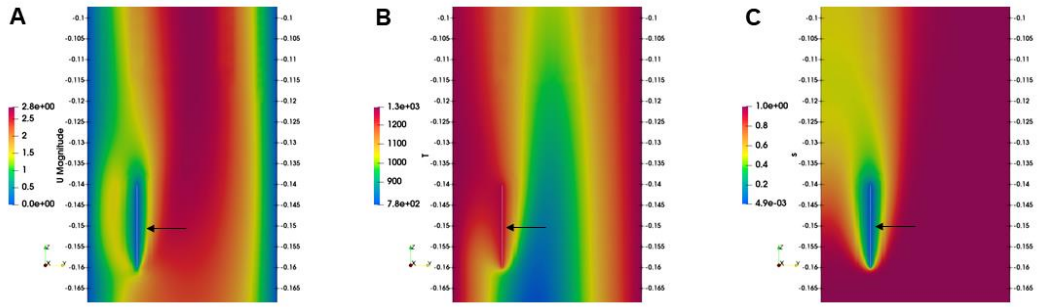

Figure S13. *YZ* slices (axes in m, at x = 0 m) through the reactor tube showing gas mag(U) (ms^{-1}), T (K), and, CH_4 distribution (s) around the 50 μm foil for an experiment with the average inlet velocity of **condition A** reduced to 1/3. Arrows indicate foil location.

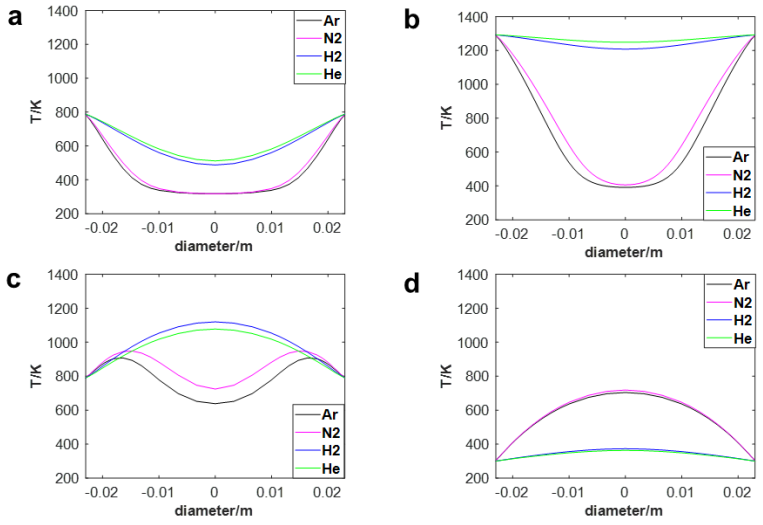

Figure S14A. Line profiles along the tube x diameter at different z values: (A) -0.2 m, (B) 0.0 m (center of hot-zone and foil position), (C) 0.2 m, and (D) 0.6 m.

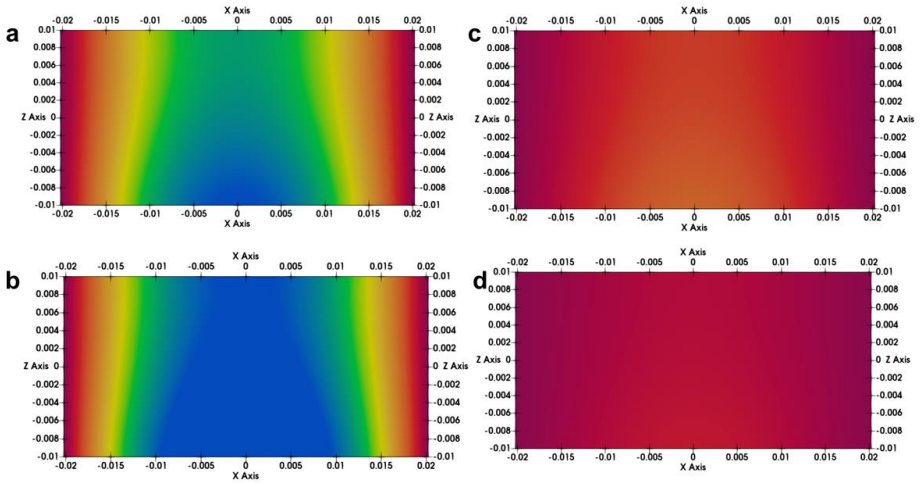

Figure S14B. Foil temperatures (K) in different gas environments (A) Ar, (B) N_2, (C) H_2, (D) He. All axes are in m.

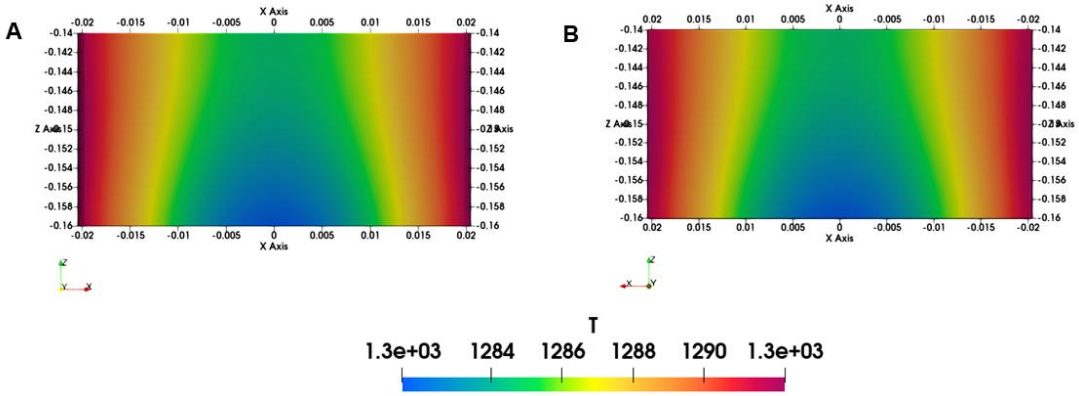

Figure S15. *T*(K) fields of the (A) bottom, and the (B) top surfaces of a 1 mm thick foil (axes in m, **foil setup A**, **condition A**).

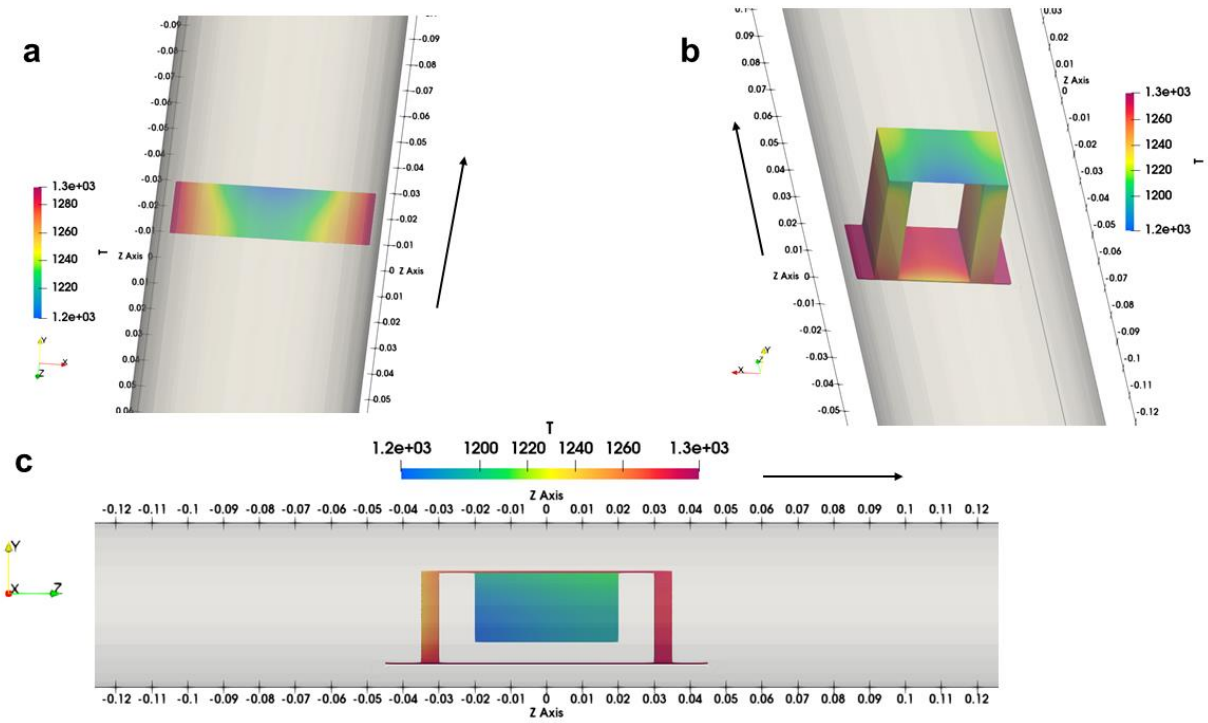

Figure S16A. Different foil positions and orientations: (A) freely suspended, (B) suspended horizontally on a holder, (C) suspended vertically on a holder. Gas flow is in the *z* direction. All axes are in m, *T* is in K.

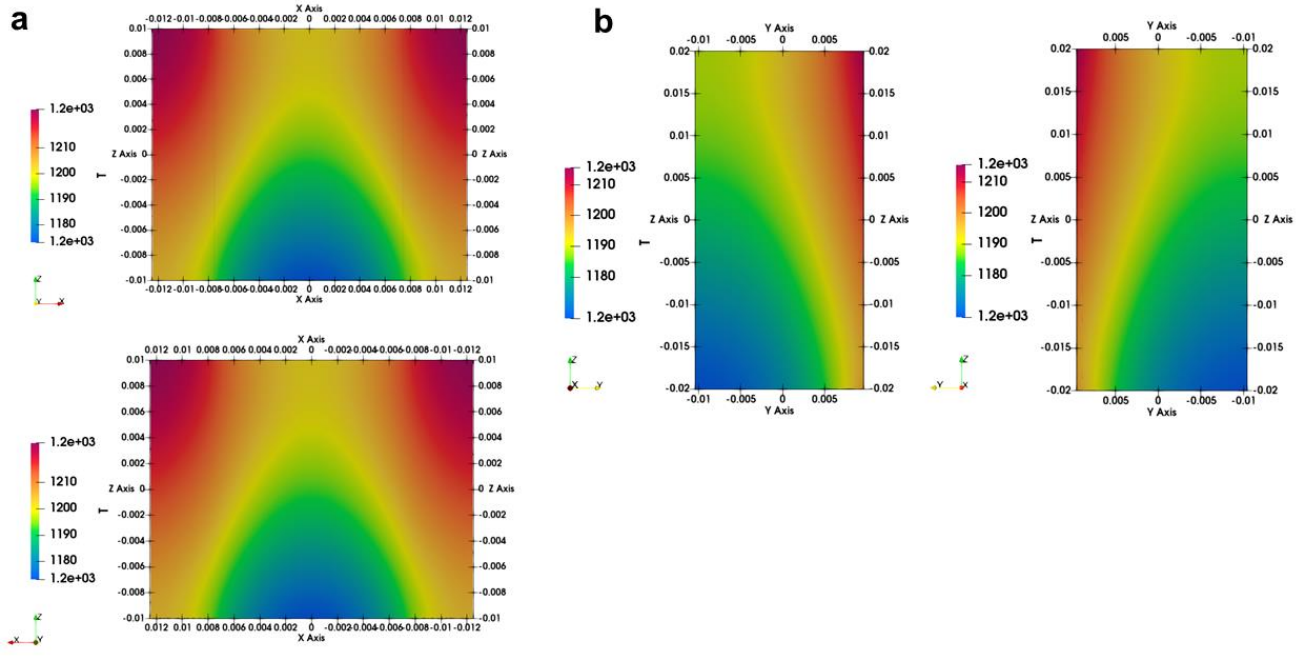

Figure S16B. Comparison of the two surfaces of a 100 μm thick copper foil on a (A) horizontal quartz holder, (B) vertical quartz holder. All axes are in m, *T* is in K.

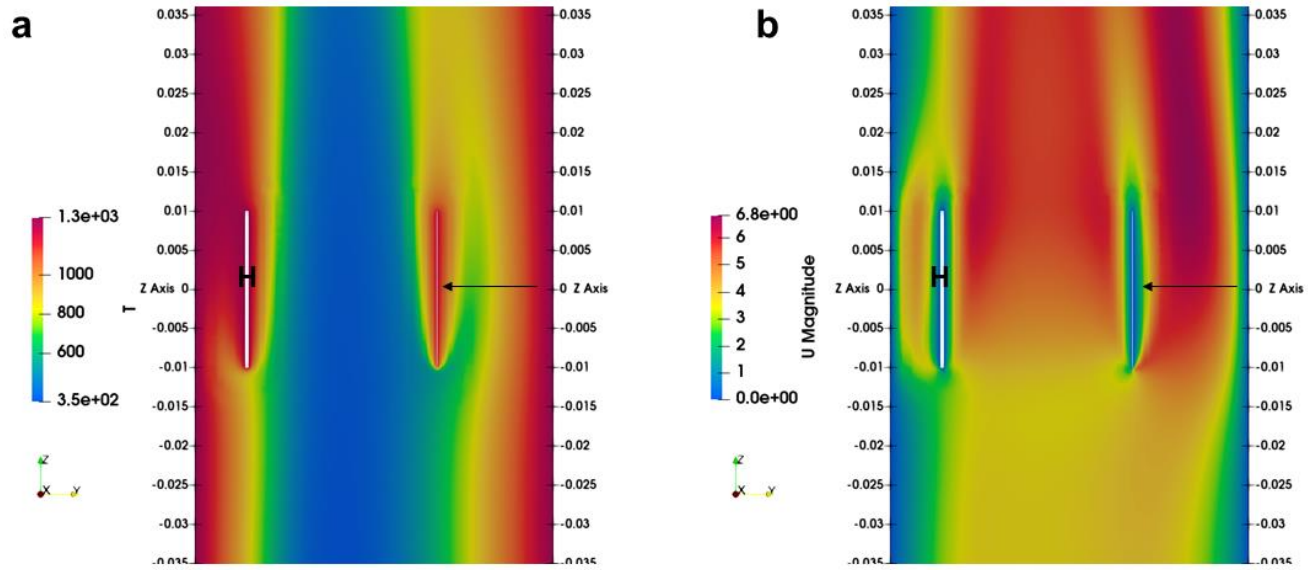

Figure S16C. *T* (K) and mag(*U*) (ms^{-1}) around a foil (indicated by an arrow) on a horizontal holder (H). All axes are in m.

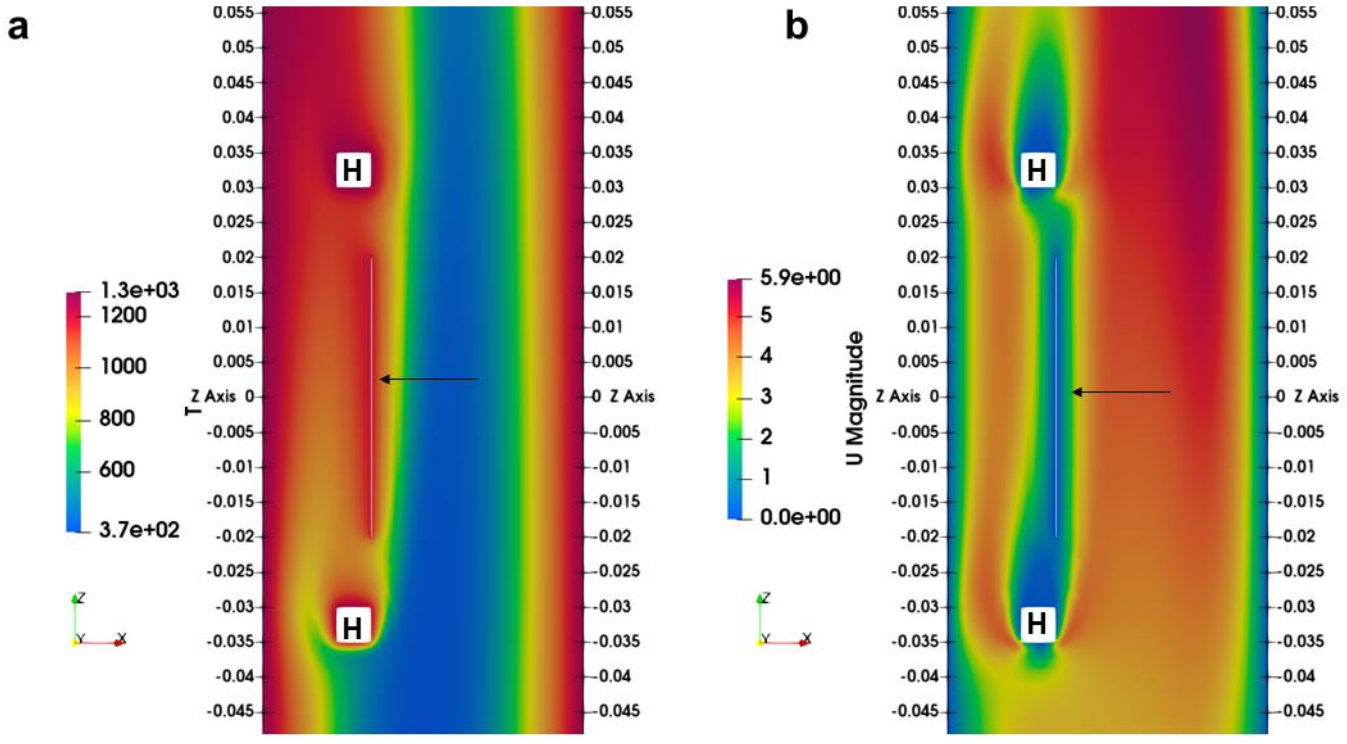

Figure S16D. *T* (K) and mag(*U*) (ms^{-1}) around a foil (indicated by an arrow) on a vertical holder (H). All axes are in m.

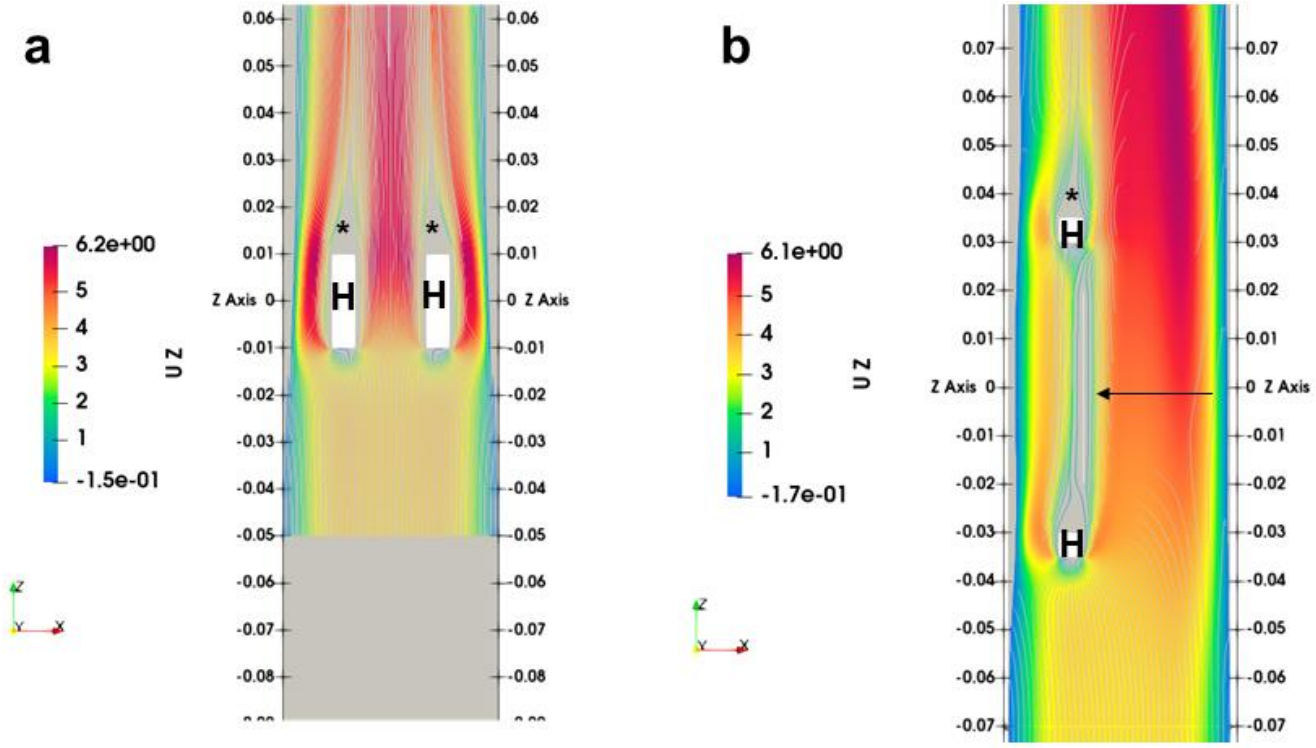

Figure S16E. Flow streamlines (color coded with U_z, ms^{-1}) around a foil (indicated by an arrow) on a (A) horizontal, and (B) a vertical holder. * indicates dead zones, H indicates holder. All axes are in m.

Tables Supplementing Main Text

Table S1. Reynolds and Mach numbers at 20 °C (293 K) for an Ar flow at 100 torr.

	U_{avg} (ms^{-1})	*Ma*	*Re*
reactor tube	1.11	0.0035	492
inlet	146.61	0.4567	5654

Table S2. Different system parameters.

	U_{avg} (ms^{-1}) at inlet	Ar (mole fraction)	H_2 (mole fraction)	Temperature	Pressure (torr)
condition T0	146.61	1	0	RT (293 K)	100
condition T1	146.61	1	0	thermal profile A applied to wall	100
condition T2	$6.4e^{-6}$	1	0	thermal profile A applied to wall	0.1
condition A	146.61	0.8035	0.1965	thermal profile A applied to wall	100

Table S3. Fields for a heated reactor tube, with and without foil for an Ar only flow (**condition T1**).

	T_{gas}, min (K)	T_{gas}, max (K)	T_{gas}, avg (K)	T_{foil}, min (K)	T_{foil}, min (K)	T_{foil}, avg (K)
with foil	392.694	1292.3	722.249	1202.51	1292.3	1245.54
without foil	393.159	1292.3	709.162	-	-	-

	U, avg (ms^{-1})	k, avg (m^2s^{-2})	Ti, avg (%)
with foil	3.49	0.0079	2.08
without foil	3.34	0.0077	2.15

Table S4. Effect of different heating modes on foil temperature (100 μm foil with **condition T1** except for the last simulation with **condition T2**).

Heating Modes	Foil Set-Up	T_{foil} min (K)	T_{foil} max (K)	T_{foil} avg (K)	T_{gas} min (K)	T_{gas} avg (K)
all modes (default)	foil edges completely touch pipe wall (**setup A**)	1202.51	1292.3	1245.54	392.694	722.249
no radiation (control H1)	foil edges completely touch pipe wall, radiation turned off	1196.28	1292.3	1241.64	392.747	722.122
no conduction (control H2)	2 mm gap between foil edges and pipe wall	960.735	991.215	978.753	392.564	713.408
partial conduction (control H3)	upstream half of the foil touches the wall, 2 mm gap between downstream half and wall	1181.95	1292.3	1218.43	393.547	722.582
partial conduction (control H4)	upstream half of the foil touches the wall, 1 mm gap between downstream half and wall	1184.74	1292.3	1222.2	393.14	721.836
no convection (control H5, condition T2)	foil edges completely touch pipe wall (**setup A**)	1291.86	1292.3	1292.22	1291.1	1291.7

Heating Modes	U, avg (ms^{-1})	k, avg (m^2s^{-2})	Ti, avg (%)
all modes (default)	3.49	0.0079	2.08
no radiation (control H1)	3.49	0.008	2.08
no conduction (control H2)	3.43	0.008	2.09
partial conduction (control H3)	3.48	0.008	2.09
partial conduction (control H4)	3.58	0.008	2.03
no convection (control H5, condition T2)	0.0003	-	-

Table S5. Effect of process gas composition with an inlet U_{avg} of (A) 146.61 and (B) 50.58 ms^{-1} for a 100 μm foil.

(A)

Mass Fraction of H_2 (%)	Mole Fraction of H_2 (%)	T_{foil} min (K)	T_{foil} max (K)	T_{foil} avg (K)	hot-zone T_{gas}, min (K)	hot-zone T_{gas}, max (K)	hot-zone T_{gas}, avg (K)
0.0	0.0	1202.51	1292.3	1245.54	392.694	1292.3	722.249
1.23(**condition A**)	19.65	1196.71	1292.3	1242.75	406.764	1292.3	760.085
9.42	67.25	1204.82	1292.3	1246.91	602.354	1292.3	949.089
15.35	78.16	1217.44	1292.3	1253.36	773.379	1292.3	1038.81
100.0	100.0	1268.63	1292.3	1280.02	1186.87	1292.3	1241.96

Mass Fraction of H_2 (%)	Mole Fraction of H_2 (%)	hot-zone U, avg (ms^{-1})	hot-zone k, avg (m^2s^{-2})	hot-zone Ti, avg (%)
0.0	0.0	3.49	0.0079	2.08
1.23(**condition A**)	19.65	3.73	0.0063	1.74
9.42	67.25	4.90	0.0011	0.55
15.35	78.16	5.45	0.00025	0.24
100.0	100.0	6.69	9.46e-9	0.0012

(B)

Mass Fraction of H_2 (%)	Mole Fraction of H_2 (%)	T_{foil}, min (K)	T_{foil}, max (K)	T_{foil}, avg (K)	hot-zone T_{gas}, min (K)	hot-zone T_{gas}, max (K)	hot-zone T_{gas}, avg (K)
0.0	0.0	1258.69	1292.3	1275.14	705.895	1292.3	1012
6.31	56.96	1274.62	1292.3	1283.02	1070.35	1292.3	1186.92
14.65	77.22	1284.26	1292.3	1288.05	1219.14	1292.3	1258.53
100.0	100.0	1290.6	1292.3	1291.37	1284.22	1292.3	1288.74

Mass Fraction of H_2 (%)	Mole Fraction of H_2 (%)	hot-zone U, avg (ms^{-1})	hot-zone k, avg (m^2s^{-2})	hot-zone Ti, avg (%)
0.0	0.0	1.79	3.38e-5	0.26
6.31	56.96	2.19	2.3e-7	0.018
14.65	77.22	2.35	1.03e-10	0.00035
100.0	100.0	2.45	1e-15	1.05e-6

Table S6. Effect of H_2 proportion and inlet gas velocity for a 100 μm foil.

U_{avg} (ms^{-1}) at inlet	T_{foil} avg (K)	hot-zone T_{gas}, min (K)	hot-zone T_{gas}, max (K)	hot-zone T_{gas}, avg (K)
50.58	1283.02	1070.35	1292.3	1186.92
66.58	1272.54	802.388	1292.3	1056.9
98.59	1256.01	507.893	1292.3	888.378
146.61	1242.75	406.764	1292.3	760.085
208.07	1232.44	384.109	1292.3	679.59
242.63	1227.71	381.397	1292.3	652.325

U_{avg} (ms^{-1}) at inlet	hot-zone U, avg (ms^{-1})	hot-zone k, avg (m^2s^{-2})	hot-zone Ti , avg (%)
50.58	2.19	2.30e-7	0.018
66.58	2.51	3.38e-5	0.189
98.59	3.03	0.00099	0.847
146.61	3.73	0.0063	1.741
208.07	4.62	0.0197	2.480
242.63	5.12	0.0306	2.789

Table S7. Effect of H_2 proportion and inlet gas velocity for a 50 μm foil.

U_{avg} (ms^{-1}) at inlet	Mole Fraction of Ar	T_{foil} min (K)	T_{foil} max (K)	T_{foil} avg (K)	hot-zone T_{gas}, min (K)	hot-zone T_{gas}, max (K)	hot-zone T_{gas}, avg (K)
50.58	0.43 (**condition A1**)	1262.67	1292.3	1277.02	1064.19	1292.3	1180.39
66.58	0.57 (**condition A2**)	1227.9	1292.3	1259.48	794.291	1292.3	1050.33
146.61	0.8035 (**condition A**)	1132.96	1292.3	1210.12	406.519	1292.3	761.253
242.63	0.88 (**condition A3**)	1089.16	1292.3	1185.73	382.415	1292.3	652.382

U_{avg} (ms^{-1}) at inlet	hot-zone U, avg (ms^{-1})	hot-zone k , avg (m^2s^{-2})	hot-zone Ti, avg (%)
50.58	2.18	3.24e-7	0.021
66.58	2.49	3.97e-5	0.206
146.61	3.71	0.0064	1.75
242.63	5.13	0.028	2.81

Table S8. Different process gases (average inlet velocity of 146.61 ms^{-1} at 100 torr with a 2 cm x 4 cm and 100 μm thick Cu foil suspended at the center (z = 0, foil setup B) of the tube reactor).

	T_{foil}, min (K)	T_{foil}, max (K)	T_{foil}, avg (K)	hot-zone T_{gas}, min (K)	hot-zone T_{gas}, max (K)	hot-zone T_{gas}, avg (K)
H_2	1268.96	1292.3	1280.19	1187.35	1292.3	1245.18
He	1280.91	1292.3	1286.38	1234.2	1292.3	1267.19
N_2	1164.24	1292.3	1225.78	381.914	1292.3	798.108
Ar (condition T1)	1198.26	1292.3	1243.15	352.37	1292.3	723.584

	hot-zone U, avg (ms^{-1})	hot-zone k, avg (m^2s^{-2})	hot-zone Ti, avg (%)
H_2	6.67	$1.35e^{-10}$	0.00014
He	6.83	$8.11e^{-12}$	$3.4e^{-5}$
N_2	3.88	0.0018	0.9
Ar (condition T1)	3.43	0.0032	1.34

Table S9. Effect of variation in foil thickness

(A) condition A

Thickness/ μm	T_{foil} min (K)	T_{foil} max (K)	T_{foil} avg (K)	hot-zone T_{gas}, min (K)	hot-zone T_{gas}, max (K)	hot-zone T_{gas}, avg (K)
1000	1281.45	1292.3	1286.73	407.839	1292.3	766.574
500	1270.75	1292.3	1281.15	407.608	1292.3	761.651
300	1257.17	1292.3	1274.03	407.62	1292.3	762.03
200	1241.50	1292.3	1265.88	408.369	1292.3	762.631
100	1196.71	1292.3	1242.75	406.764	1292.3	760.085
50	1132.96	1292.3	1210.12	406.519	1292.3	761.253

Thickness/ μm	hot-zone U, avg (ms^{-1})	hot-zone k, avg (m^2s^{-2})	hot-zone Ti, avg (%)
1000	3.81	0.0064	1.71
500	3.78	0.0064	1.73
300	3.76	0.0064	1.73
200	3.75	0.0064	1.74
100	3.73	0.0063	1.74
50	3.71	0.0064	1.75

(B) for an inlet U_{avg} of 50.58 ms^{-1} and mole fractions of 0.57 H_2 and 0.43 of Ar at 100 torr

Thickness/ μm	T_{foil} min (K)	T_{foil} max (K)	T_{foil} avg (K)	hot-zone T_{gas}, min (K)	hot-zone T_{gas}, max (K)	hot-zone T_{gas}, avg (K)
100	1274.62	1292.3	1283.02	1070.35	1292.3	1186.92
50	1262.67	1292.3	1277.02	1064.19	1292.3	1180.39

(C) for an inlet U_{avg} of 242.64 ms^{-1} and mole fractions of 0.88 Ar, 0.12 H_2 at 100 torr

Thickness/ μm	T_{foil} min (K)	T_{foil} max (K)	T_{foil} avg (K)	hot-zone T_{gas}, min (K)	hot-zone T_{gas}, max (K)	hot-zone T_{gas}, avg (K)
100	1169.3	1292.3	1227.71	381.397	1292.3	652.325
50	1089.16	1292.3	1185.73	382.415	1292.3	652.382

Table S10A. Quartz holders (centered at z = 0) with horizontally and vertically suspended 100 μm foils, and condition A.

Substrate Holder	T_{foil}, min (K)	T_{foil}, max (K)	T_{foil}, avg (K)	T_{gas}, min (K)	T_{gas}, max (K)	T_{gas}, avg (K)
None	1198.26	1292.3	1243.15	352.37	1292.3	723.584
Horizontal	1172.85	1225.12	1202.51	360.363	1292.3	817.764
Vertical	1166.43	1215.36	1188.26	359.334	1292.3	793.74

Substrate Holder	U, avg (ms^{-1})	k, avg (m^2s^{-2})	Ti, avg (%)
None	3.43	0.003	1.34
Horizontal	4.74	0.0026	0.88
Vertical	4.15	0.0025	0.99

Table S10B. Holders (centered at z = 0) with horizontally suspended foils and condition A.

	T_{foil}, min (K)	T_{foil}, max (K)	T_{foil}, avg (K)	T_{gas}, min (K)	T_{gas}, max (K)	T_{gas}, avg (K)
Quartz	1172.85	1225.12	1202.51	360.363	1292.3	817.764
Alumina	1165.99	1217.4	1195.26	360.387	1292.3	815.527
Tungsten	1202.59	1237.1	1234.39	360.366	1292.3	819.184

	U, avg (ms^{-1})	k, avg (m^2s^{-2})	Ti, avg (%)
Quartz	4.74	0.0026	0.88
Alumina	4.73	0.0026	0.88
Tungsten	4.75	0.0026	0.88

References

(1) Greenshields, C.; Weller, H. *Notes on computational fluid dynamics*:*General principles*; CFD Direct Ltd, 2022.

(2) OpenFOAM. *OpenFOAM v2006*. https://www.openfoam.com/news/main-news/openfoam-v2006.

(3) Minkowycz, W. J.; Sparrow, E. M.; Murthy, J. Y., Eds. *Handbook of Numerical Heat Transfer*; Wiley, 2000. DOI: 10.1002/9780470172599.

(4) Vortmeyer, D.; Kabelac, S. K3 Gas Radiation: Radiation from Gas Mixtures. In *VDI Heat Atlas*; Springer, Berlin, Heidelberg, 2010; pp 979–988. DOI: 10.1007/978-3-540-77877-6_66.

(5) Biswajit Banerjee. An evaluation of plastic flow stress models for the simulation of high-temperature and high-strain-rate deformation of metals. DOI: 10.13140/RG.2.1.4289.9285.

(6) National Bureau of Standards. *THERMAL CONDUCTIVITY OF ALUMINUM, COPPER, IRON, AND TUNGSTEN FOR TEMPERATURES FROM1 K TO THE MELTING POINT*, 1984.

(7) https://www.omnicalculator.com/physics/mean-free-path.